

Hybrid stars in the light of the merging event GW170817

ALESSANDRO PARISI,¹ C. VÁSQUEZ FLORES,² C. HENRIQUE LENZI,³ CHIAN-SHU CHEN,¹ AND GERMÁN LUGONES⁴

¹*Department of Physics, Tamkang University, New Taipei 251, Taiwan,*

²*Centro de Ciências Exatas, Naturais e Tecnológicas, UEMASUL,
Rua Godofredo Viana 1300, Centro CEP: 65901-480, Imperatriz, Maranhão, Brazil,*

³*Department of Physics, Instituto Tecnológico de Aeronautica, DCTA, 12228-900, São José dos Campos, SP, Brazil*

⁴*Universidade Federal do ABC, Centro de Ciências Naturais e Humanas, Avenida dos Estados, 5001,
CEP 09210-170, Santo André, SP, Brazil*

ABSTRACT

We study quark-hadron hybrid stars with sharp phase transitions assuming that phase conversions at the interface are slow. Hadronic matter is described by a set of equations of state (EoS) based on the chiral effective field theory and quark matter by a generic bag model. Due to slow conversions at the interface, there is an extended region of stable hybrid stars with central densities above the density of the maximum mass star. We explore systematically the role of the transition pressure and the energy-density jump $\Delta\epsilon$ at the interface on some global properties of hybrid stars, such as the maximum mass, the last stable configuration, and tidal deformabilities. We find that for a given transition pressure, the radius of the last stable hybrid star decreases as $\Delta\epsilon$ raises resulting in a larger extended branch of stable hybrid stars. Contrary to purely hadronic stars, the tidal deformability Λ can be either a decreasing or an increasing function of the stellar mass M and for large values of the transition pressure has a very weak dependence on M . Finally, we analyze the tidal deformabilities Λ_1 and Λ_2 for a binary system with the same chirp mass as GW170817. In the scenario where at least one of the stars in the binary is hybrid, we find that models with low enough transition pressure are inside the 90% credible region of GW170817. However, these models have maximum masses below $2 M_\odot$, in disagreement with observations. We also find that the LIGO/Virgo constrain (at 90% level) and the $2 M_\odot$ requirement can be simultaneously fulfilled in a scenario where all hybrid configurations have masses larger than $1.6 M_\odot$ and the hadronic EoS is not too stiff, such as several of our hybrid models involving a hadronic EoS of intermediate stiffness. In such scenario hybrid stars may exist in Nature but both objects in GW170817 were hadronic stars.

Keywords: neutron star — tidal deformation — phase transition

1. INTRODUCTION

The composition and properties of neutron stars (NSs), which are among the densest objects in the universe, are not well understood theoretically. However, measurements of the masses or radii of these objects can strongly constrain the NS matter equation of state (EoS), and consequently the interior composition of NSs (see Lattimer (2012), and Lattimer & Prakash (2016) for a complete review).

The EoS is not only a key ingredient in modeling compact star formation, but it is also sensitive to the gravitational wave signal from mergers of binary NSs (Abbott et al. 2017). The most stringent constraints for the EoS comes from the two solar mass limit of the pulsars PSR J1614-2230 (Demorest et al. 2010), PSR J0348+0432

(Antoniadis et al. 2013), PSR J0740+6620 (Cromartie et al. 2019), and PSR J2215-5135 (Linares et al. 2018).

Another source of observational data is coming from the Neutron Star interior Composition Explorer (NICER) experiment by NASA. NICER has provided a simultaneous measurement of both mass and radius of the millisecond-pulsar PSR J0030+0451 and also inferred some thermal properties of hot regions present in the star (Riley et al. 2019; Miller et al. 2019).

New limits on the EoS were posed by the LIGO/Virgo detection of gravitational waves (GWs) originating from the NS-NS merger event GW170817 (Abbott et al. 2017), which allowed determining the tidal deformabilities of the stars involved in the collision (Annala et al. 2018; Fattoyev et al. 2018; Most et al. 2018; Raithel et al. 2018). During the inspiral phase of a NS-NS merger,

strong tidal gravitational fields deform the multipolar structure of the NSs, leaving a detectable imprint on the observed gravitational waveform of the merger (Abbott et al. 2017; Zhao & Lattimer 2018). This effect can be quantified in terms of the so-called dimensionless tidal deformability of the star, defined as:

$$\Lambda_i = \frac{2}{3} k_2^{(i)} \left(\frac{c^2 R_i}{GM_i} \right)^5, \quad (1)$$

where $k_2^{(i)}$ is the second Love number, R_i the radius, and M_i the mass of the i -th star (Flanagan & Hinderer 2008). Λ_i describes the amount of induced mass quadrupole moment when reacting to a certain external tidal field (see Hinderer (2008) and Damour & Nagar (2009) for more details).

Previously, several authors have studied tidal effects trying to impose some constraints on the EoS (Tews et al. 2018; Malik et al. 2018; De et al. 2018; Carson et al. 2019; Souza et al. 2020). Some works analyzed the tidal properties of NSs using relativistic mean-field models (Nandi et al. 2019; Lourenço et al. 2019) and Skyrme-type models (Kim et al. 2018; Tsang et al. 2019; Lourenço et al. 2020). Other focused on the role of the symmetry energy $E_{\text{sym}}(\rho)$ (Krastev & Li 2019) and analyzed the role of the appearance of Δ -isobars taking into account the data from GW170817 (Li & Sedrakian 2019).

Among the open questions that may be explored with GW measurements, the possible appearance of quark matter in compact stars is an issue that has attracted the attention for decades. In fact, it has been conjectured long ago (Ivanenko & Kurdgelaidze 1965; Pacini 1966; Itoh 1970) that a higher density class of compact stars may arise in the form of hybrid stars or quark stars (Qs), whose core or entire volume consists of quark matter (see also Mannarelli et al. (2014, 2015); Lugones (2016) and references therein). Nowadays, it is generally believed that deconfined quarks may exist inside the core of compact stars, which corresponds to the high-density and low-temperature region of the QCD phase diagram.

When considering the possibility of a phase transition from hadronic matter to quark matter in compact star interiors, it is possible that *mass twins* arise in the mass-radius diagram. The term mass twins refers to the existence of doublets (and sometimes multiplets) of stellar configurations that have the same gravitational mass but different radii. The appearance of twins may be related to the occurrence of a third family of compact stars, besides white dwarfs and ordinary NSs, which is separated from the latter by an unstable branch in the mass-radius diagram. As already discussed by Gerlach (1968), the third family is related to the behavior of the

high-density EoS, which may exhibit a phase transition. The transition to quark matter or to pion condensed matter has been considered in the context of a third family of stars by Kämpfer (1983), and later this problem was taken up again by Schertler et al. (2000) and Glendenning & Kettner (2000). EoS with multiple phases, which include a deconfined quark-matter segment, were studied recently by Alford et al. (2013, 2015); Buballa et al. (2014); Benić et al. (2015); Ranea-Sandoval et al. (2016); Kaltenborn et al. (2017); Christian et al. (2018) (see also Baym et al. (2018) for a recent review). An additional phase transition in the quark core can lead to a fourth family of compact stars (Alford & Sedrakian 2017), but we do not consider this possibility here. The influence of strong magnetic fields in hybrid stars, composed by hadrons and a pure quark matter core was recently studied in Mariani et al. (2019). According to general relativistic simulations of merging NSs including quarks at finite temperatures (Most et al. 2019), the phase transition would lead to a post-merger signal considerably different from the one expected from the inspiral, that can only probe the hadronic part of the EoS.

Besides the standard mass twins and multiplets described before, it has been shown recently that there is another mechanism that gives rise to an additional family of twins. In fact, in the case of hybrid stars having *slow* quark-hadron conversion rates at the interface, there exists a new connected extended stable branch beyond the maximum mass star, for which $\partial M/\partial \epsilon_c < 0$ (Flores, Lenzi & Lugones 2012; Pereira, Flores & Lugones 2018; Mariani et al. 2019). In this paper we focus on the consequences of a potential appearance of a sharp hadron-quark phase transition in the interior of NSs paying particular attention to the role of slow phase conversions. We investigate the possibility of recognizing hybrid star branches by observing tidal deformations and examine how well future binary neutron star observations can possibly constrain the properties of the phase transition.

This paper is organized as follows. In Sec. 2, we describe the hadronic and quark matter EoSs used in this work and combine them in order to obtain hybrid EoSs with sharp first order phase transitions at some given pressures. In Sec. 3 we summarize the role of slow transitions on the dynamical stability of hybrid stars and in Sec. 4 we present the equations for the tidal deformability used in the calculations. In Sec. 5 we present our results for the tidal deformations of hybrid stars. In Sec. 6 we present our main conclusions.

2. EQUATIONS OF STATE

In this section, we discuss the cold dense-matter models we use in our analysis. In Sec. 2.1 we describe the hadronic model, in Sec. 2.2 the quark matter model, and in Sec. 2.3 we explain the procedure used to construct first order phase transitions with a sharp density discontinuity.

2.1. Hadronic Matter

For the hadronic phase (HP) we use a model presented by Hebel et al. (2013), which is based on nuclear interactions derived from chiral effective field theory (EFT). In recent years, the development of chiral EFT has provided the framework for a systematic expansion for nuclear forces at low momenta, allowing one to constrain the properties of neutron-rich matter up to nuclear saturation density to a high degree.

However, our knowledge of the EOS at densities greater than 1 to 2 times the nuclear saturation density is still insufficient due to limitations on both laboratory experiments and theoretical methods. The EoS at supranuclear densities is described by a set of three polytropes which are valid, respectively, in three consecutive density regions. For these polytropic EoSs it is required non-violation of causality and consistence with the recently observed pulsars with $\sim 2M_\odot$ (Demorest et al. 2010; Antoniadis et al. 2013). In Hebel et al. (2013) is possible to find numerical tables for three representative EoS labeled as soft, intermediate and stiff.

To describe the structure of the crust we follow the formalism developed by Baym et al. (1971) for the outer crust, while we employ the pioneering work of Negele & Vautherin (1973) for the description of the inner crust.

2.2. Quark Matter

For the quark phase (QP) we adopt the generic bag model presented in Alford et al. (2005), which is defined by the following grand thermodynamic potential

$$\Omega_{\text{QM}} = -\frac{3}{4\pi^2}a_4\mu^4 + \frac{3}{4\pi^2}a_2\mu^2 + B_{\text{eff}} + \Omega_e, \quad (2)$$

where $\mu \equiv (\mu_u + \mu_d + \mu_s)/3$ is the quark chemical potential, B_{eff} , a_4 , and a_2 are three free parameters independent of μ , and Ω_e is the grand thermodynamic potential for electrons e . For hybrid systems, though, it happens that the contribution to the thermodynamic quantities coming from electrons is negligible (see discussion in Pereira, Flores & Lugones (2018)). The influence of strong interactions on the pressure of the free-quark Fermi sea is roughly taken into account by the parameter a_4 , where $0 \leq a_4 \leq 1$, and $a_4 = 1$ indicates no correction to the ideal gas. The effect of the color superconductivity phenomenon in the Color Flavor Locked

(CFL) phase can be explored setting $a_2 = m_s^2 - 4\Delta^2$, being m_s the mass of the strange quark and Δ the energy gap associated with quark pairing. The standard MIT bag model is obtained for $a_4 = 1$ and $a_2 = m_s^2$. The bag constant B_{eff} is related to the confinement of quarks, representing in a phenomenological way the vacuum energy (see Farhi & Jaffe (1984)). From Eq. (2), one can obtain the pressure $p = -\Omega_{\text{QM}}$, the baryon number density

$$n = -\frac{1}{3} \frac{\partial \Omega_{\text{QM}}}{\partial \mu} = \frac{1}{2\pi^2}(2a_4\mu^3 - a_2\mu), \quad (3)$$

and the energy density

$$\begin{aligned} \epsilon &= 3n\mu - p = \frac{9}{4\pi^2}a_4\mu^4 - \frac{3}{4\pi^2}a_2\mu^2 + B_{\text{eff}} \\ &= 3p + 4B_{\text{eff}} + \frac{3a_2}{2\pi^2}\mu^2. \end{aligned} \quad (4)$$

An analytic expression of the form $p = p(\epsilon)$ for this phenomenological model can be simply obtained if one solves Eq. (4) for μ and replaces it in Eq. (2). The final result is

$$p(\epsilon) = \frac{(\epsilon - 4B_{\text{eff}})}{3} - \frac{a_2^2}{12\pi^2 a_4} \left[1 + \sqrt{1 + \frac{16\pi^2 a_4}{a_2^2}(\epsilon - B_{\text{eff}})} \right]. \quad (5)$$

2.3. Phase Transitions

The density at which the hadron-quark phase transition occurs is not known, but it is expected to occur at some times the nuclear saturation density. In a NS, such a transition can lead to two possible types of internal structure, depending on the surface tension between hadronic and quark matter (Iida & Sato 1998; Endo 2011). If the surface tension between hadronic and quark matter is larger than a critical value, which is estimated to be around 60 MeV/fm² (Voskresensky et al. 2003; Maruyama et al. 2007), then there is a sharp interface and we have a Maxwell phase transition. If the surface tension is below the critical value, then there is a mixed phase of matter between pure nuclear and pure quark regimes usually called Gibbs phase transition. In this work we assume that the interface between hadronic and quark matter is a sharp interface, which is a possible scenario given the uncertainties in the value of the surface tension (Pinto et al. 2012; Lugones et al. 2013; Lugones & Grunfeld 2013, 2019).

At the quark-hadron interface the following conditions are verified:

- the pressure is continuous (mechanical equilibrium):

$$p_{\text{tr}}^{\text{QP}} = p_{\text{tr}}^{\text{HP}} \equiv p_{\text{tr}}. \quad (6)$$

Table 1. We list our choices for the parameters a_2 , p_{tr} and $\Delta\epsilon$, which according to the discussion given in Sec. 2.3, define the localisation of the quark-hadron interface as well as the parameters B_{eff} and a_4 of the quark matter EoS. In this Table it is assumed that the hadronic EoS is described by the *soft* model of Hebeler et al. (2013). For completeness we include the maximum stellar mass M_{max} of each model.

Model	$p_{\text{tr}}(\text{MeV}/\text{fm}^3)$	$\epsilon_{\text{tr}}^{\text{HP}}(\text{MeV}/\text{fm}^3)$	$n_{\text{B, tr}}^{\text{HP}}(\text{fm}^{-3})$	$\Delta\epsilon(\text{MeV}/\text{fm}^3)$	$a_2^{1/2}(\text{MeV})$	$B_{\text{eff}}^{1/4}(\text{MeV})$	a_4	$M_{\text{max}}(M_{\odot})$
1	77.9	585.2	0.592	60	100	164.79	0.976	1.497
2	124.3	640.7	0.639	50	100	153.15	0.848	1.666
3	124.3	640.7	0.639	120	100	161.75	0.919	1.640
4	124.3	640.7	0.639	200	100	170.15	0.999	1.565
5	165.5	719.1	0.704	100	100	153.35	0.837	1.490
6	165.5	719.1	0.704	250	100	170.30	0.960	1.564
7	242.8	844.6	0.799	300	100	163.89	0.856	1.724
8	242.8	844.6	0.799	400	100	173.85	0.916	1.714
9	242.8	844.6	0.799	500	100	182.34	0.976	1.712
10	359.8	1004	0.912	500	100	163.87	0.783	1.866
11	359.8	1004	0.912	700	100	182.33	0.865	1.865
12	359.8	1004	0.912	900	100	196.45	0.947	1.865
13	485.8	1154	1.008	600	100	146.29	0.671	1.947
14	485.8	1154	1.008	800	100	170.35	0.730	1.946
15	485.8	1154	1.008	1000	100	187.13	0.788	1.946

- The energy density has a jump $\Delta\epsilon$, i.e.:

$$\epsilon_{\text{tr}}^{\text{QP}} = \epsilon_{\text{tr}}^{\text{HP}} + \Delta\epsilon. \quad (7)$$

- The Gibbs free energy per baryon at zero temperature, $g = (p + \epsilon)/n$, is continuous (chemical equilibrium):

$$g_{\text{tr}}^{\text{QP}} = g_{\text{tr}}^{\text{HP}}. \quad (8)$$

From Eq. (4) we see that $g^{\text{QP}} = 3\mu$, and for hadronic matter we write $g^{\text{HP}} = (p^{\text{HP}} + \epsilon^{\text{HP}})/n^{\text{HP}}$. Therefore, at the interface we have:

$$3\mu_{\text{tr}} = \frac{p_{\text{tr}}^{\text{HP}} + \epsilon_{\text{tr}}^{\text{HP}}}{n_{\text{tr}}^{\text{HP}}}. \quad (9)$$

Now using Eq. (2), we can write Eq. (6) as:

$$p_{\text{tr}}^{\text{HP}} = \frac{3}{4\pi^2} a_4 \mu_{\text{tr}}^4 - \frac{3}{4\pi^2} a_2 \mu_{\text{tr}}^2 - B_{\text{eff}}. \quad (10)$$

Similarly, using Eq. (4), we can write Eq. (7) as:

$$\epsilon_{\text{tr}}^{\text{HP}} + \Delta\epsilon = 3p_{\text{tr}}^{\text{HP}} + 4B_{\text{eff}} + \frac{3a_2}{2\pi^2} \mu_{\text{tr}}^2, \quad (11)$$

where μ_{tr} is given by Eq. (9). From Eqs. (10)–(11) we can write the parameters B_{eff} and a_4 in terms of $p_{\text{tr}}^{\text{HP}}$, $\epsilon_{\text{tr}}^{\text{HP}}$, $n_{\text{tr}}^{\text{HP}}$, μ_{tr} , $\Delta\epsilon$, and a_2 in the form:

$$\begin{cases} B_{\text{eff}} = \beta_0 + \beta_1 \Delta\epsilon + \beta_2 a_2 \\ a_4 = \alpha_0 + \alpha_1 \Delta\epsilon + \alpha_2 a_2 \end{cases} \quad (12)$$

with

$$\beta_0 = \frac{1}{4}(\epsilon_{\text{tr}}^{\text{HP}} - 3p_{\text{tr}}^{\text{HP}}), \quad \beta_1 = \frac{1}{4}, \quad \beta_2 = -\frac{3\mu_{\text{tr}}^2}{8\pi^2},$$

$$\alpha_0 = \frac{\pi^2}{3\mu_{\text{tr}}^4}(\epsilon_{\text{tr}}^{\text{HP}} + p_{\text{tr}}^{\text{HP}}), \quad \alpha_1 = \frac{\pi^2}{3\mu_{\text{tr}}^4}, \quad \alpha_2 = \frac{1}{2\mu_{\text{tr}}^2}.$$

These coefficients are fixed once the transition point has been chosen.

In this work we fix the parameter a_2 to the typical value $a_2^{1/2} = 100$ MeV and explore several values of the transition pressure p_{tr} and the density jump $\Delta\epsilon$ at the interface, spanning a wide range of values for these quantities. Our choices for p_{tr} and $\Delta\epsilon$ are shown in Tables 1, 2 and 3, together with other properties of matter at the discontinuity, the corresponding values of the quark matter EoS parameters, and the maximum mass M_{max} for each model. The values presented in Tables 1, 2 and 3 correspond, respectively, to the soft, intermediate and stiff hadronic EoSs of Hebeler et al. (2013). The curves of the resulting hybrid EoSs are shown in Fig. 1.

3. SLOW TRANSITIONS AND DYNAMICAL STABILITY OF HYBRID STARS

At the interface, where the phase transition takes place, the physics of the quark-hadron reactions can be presented in two different types. Depending on their timescale they can be classified in slow and fast transitions. The slow case is present when the timescale of

Table 2. Same as in Table 1 but assuming that the hadronic EoS is described by the *intermediate* model of Hebeler et al. (2013).

Model	$p_{\text{tr}}(\text{MeV}/\text{fm}^3)$	$\epsilon_{\text{tr}}^{\text{HP}}(\text{MeV}/\text{fm}^3)$	$n_{\text{B,tr}}^{\text{HP}}(\text{fm}^{-3})$	$\Delta\epsilon(\text{MeV}/\text{fm}^3)$	$a_2^{1/2}(\text{MeV})$	$B_{\text{eff}}^{1/4}(\text{MeV})$	a_4	$M_{\text{max}}(M_{\odot})$
1	19.25	295.0	0.304	100	100	156.68	0.784	1.646
2	19.25	295.0	0.304	150	100	162.58	0.874	1.541
3	19.25	295.0	0.304	200	100	167.90	0.964	1.453
4	49.02	380.9	0.384	150	100	161.74	0.791	1.622
5	49.02	380.9	0.384	220	100	169.16	0.882	1.510
6	49.02	380.9	0.384	280	100	174.82	0.961	1.428
7	104.5	475.3	0.464	200	100	158.36	0.683	1.865
8	104.5	475.3	0.464	300	100	169.27	0.767	1.831
9	104.5	475.3	0.464	400	100	178.41	0.851	1.830
10	224.5	649.7	0.592	400	100	158.46	0.569	2.270
11	224.5	649.7	0.592	550	100	174.09	0.633	2.269
12	224.5	649.7	0.592	700	100	186.38	0.698	2.269
13	377.6	827.9	0.704	600	100	145.08	0.445	2.428
14	377.6	827.9	0.704	800	100	169.59	0.492	2.428
15	377.6	827.9	0.704	1000	100	186.56	0.540	2.428

Table 3. Same as in Table 1 but assuming that the hadronic EoS is described by the *stiff* model of Hebeler et al. (2013).

Model	$p_{\text{tr}}(\text{MeV}/\text{fm}^3)$	$\epsilon_{\text{tr}}^{\text{HP}}(\text{MeV}/\text{fm}^3)$	$n_{\text{B,tr}}^{\text{HP}}(\text{fm}^{-3})$	$\Delta\epsilon(\text{MeV}/\text{fm}^3)$	$a_2^{1/2}(\text{MeV})$	$B_{\text{eff}}^{1/4}(\text{MeV})$	a_4	$M_{\text{max}}(M_{\odot})$
1	20.39	249.2	0.256	80	100	147.08	0.622	1.852
2	20.39	249.2	0.256	130	100	154.11	0.705	1.711
3	20.39	249.2	0.256	180	100	160.28	0.789	1.596
4	52.49	302.2	0.304	100	100	142.52	0.535	2.054
5	52.49	302.2	0.304	200	100	156.81	0.645	1.825
6	52.49	302.2	0.304	300	100	168.01	0.756	1.770
7	92.63	361.4	0.352	250	100	154.54	0.547	2.318
8	92.63	361.4	0.352	300	100	160.67	0.584	2.318
9	92.63	361.4	0.352	350	100	166.17	0.621	2.317
10	152.9	448.9	0.416	300	100	147.16	0.443	2.662
11	152.9	448.9	0.416	400	100	160.35	0.489	2.661
12	152.9	448.9	0.416	500	100	170.91	0.536	2.661
13	259.1	573.6	0.496	500	100	145.66	0.359	2.874
14	259.1	573.6	0.496	600	100	159.19	0.385	2.874
15	259.1	573.6	0.496	700	100	169.95	0.411	2.874

the reactions is greater than the timescale of the oscillations. In the opposite case, when the timescale of the reactions is lower than the timescale of the oscillations, we have a fast transition. In the slow case, when fluid elements near the interface are perturbed and displaced from their equilibrium position, they maintain their composition and co-move with the motion of the interface. In this work we will focus our discussion on the consequences of slow transitions. A slow phase tran-

sition has significant consequences at the macroscopic level, when the dynamical behavior of the star against perturbations is investigated (Pereira, Flores & Lugones 2018; Mariani et al. 2019). The effect can be encoded in the junction conditions for the radial eigenfunctions ξ and Δp . In particular, in the case of slow transitions they are continuous variables, which can be written as

$$[\xi] = \xi_+ - \xi_- = 0, \quad [\Delta p] = (\Delta p)_+ - (\Delta p)_- = 0 \quad (13)$$

where $[x] \equiv x_+ - x_-$, with x_+ and x_- defined as the values after and before the interface, taking a reference system centered at the star. One direct consequence of the discontinuity conditions for the slow transition case is that the region of stable stars can be extended beyond the maximum mass point, which becomes apparent by determining the frequency of the fundamental radial oscillation mode (Flores, Lenzi & Lugones 2012; Pereira, Flores & Lugones 2018; Mariani et al. 2019). Typically, for homogeneous (one phase) stars, the frequency ω_0 of the fundamental oscillation mode verifies ($\omega_0^2 > 0$) for the dynamically stable configurations, and the last stable object has $\omega_0 = 0$. Coincidentally, the last stable star is the one that is just localized at the top of the mass versus radius curve (the maximum mass point). This fact justifies the wide use of the following static stability criterion instead of the dynamical one:

$$\frac{\partial M}{\partial \epsilon_c} < 0 \quad \Rightarrow \quad (\text{unstable configuration}), \quad (14)$$

$$\frac{\partial M}{\partial \epsilon_c} > 0 \quad \Leftarrow \quad (\text{stable configuration}). \quad (15)$$

In practice, this criterion is used to identify the last stable stellar configuration because, for a one-phase star, when $\omega_0 = 0$ the derivative $\partial M/\partial \epsilon_c$ changes its sign.

However, in the case of two-phase stars with slow conversions at the interface, zero frequency modes happen in general after the point of maximum mass (for further details see e.g. Pereira, Flores & Lugones (2018)). This gives rise to an extended region of stable hybrid stars with central densities that are larger than the density of the maximum mass star, as can be seen in Fig. 2. The last stable star, which has a zero frequency fundamental mode, has been identified in Fig. 2 with an asterisk. Notice that hybrid models with low enough transition pressure are not able to reach a maximum mass above the observed value $M_{\text{max}} \approx 2M_{\odot}$. As apparent from Fig. 2, for a given transition pressure, the largest the density jump $\Delta\epsilon$, the smallest the radius of the last stable hybrid star.

4. TIDAL DEFORMABILITY EQUATIONS

The theory of relativistic tidal effects in binary systems was obtained by Damour & Nagar (2009) and Poisson (2009), and it has been focus of intense research (Flanagan & Hinderer 2008; Fattoyev et al. 2013; Malik et al. 2018; Hornick et al. 2018; Kumar 2017; Hinderer 2010; Hinderer 2008). In this section we will merely describe our procedure for computing the important physical quantities.

The first step in order to investigate the tidal deformability of binary systems is the computation of

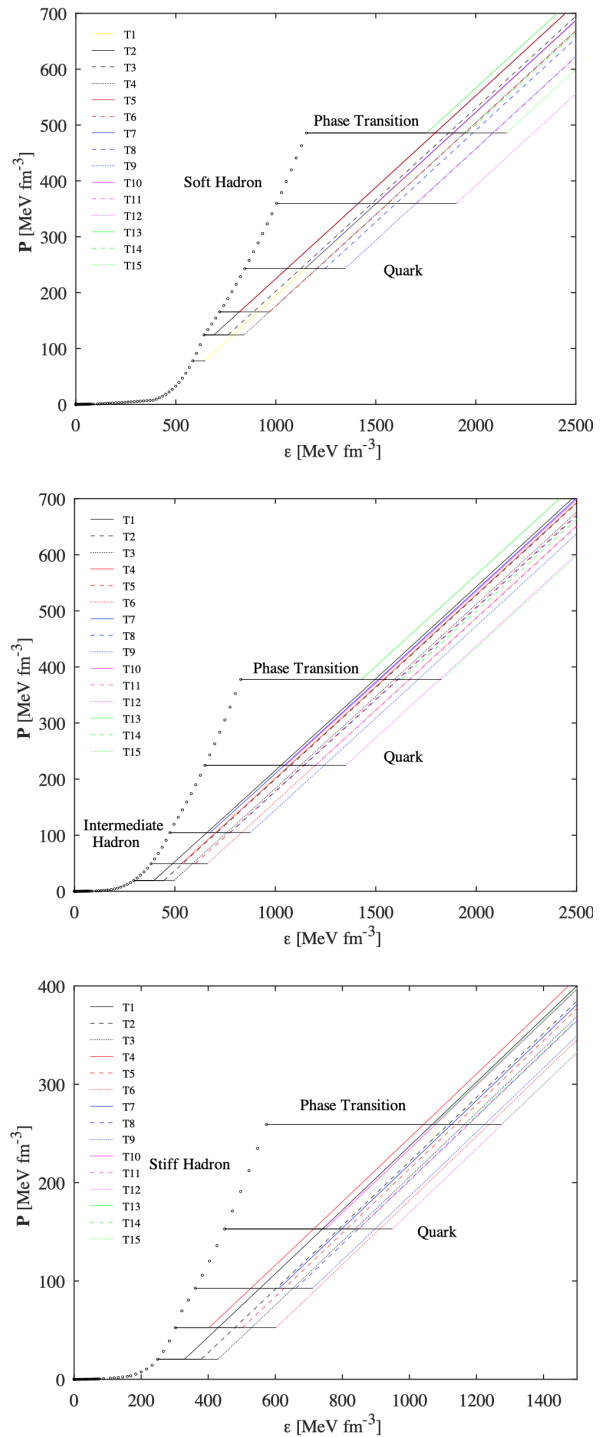


Figure 1. Hybrid EoSs used in this work. For each of the three hadronic EoS labeled as soft, intermediate and stiff we consider fifteen possible phase transitions using different values of the transition pressure p_{tr} and the density jump $\Delta\epsilon$ at the interface (see Sec. 2.3). The numerical values of the parameters for each model can be found in Tables 1, 2 and 3

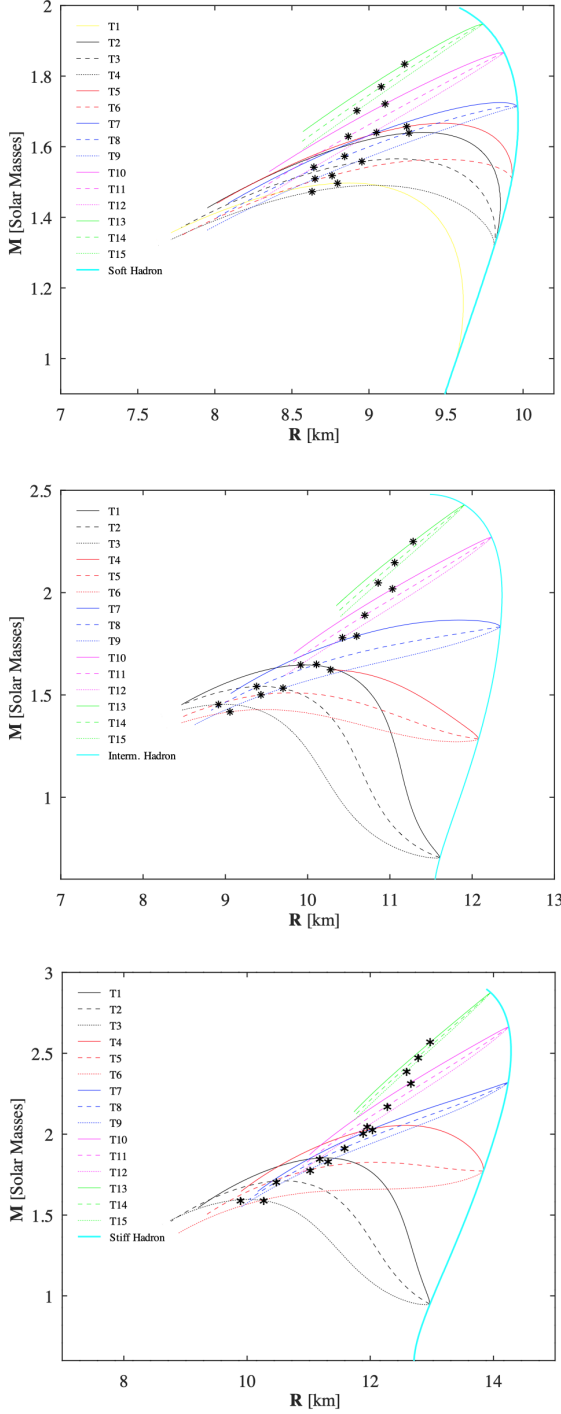


Figure 2. Mass-radius relations for the hybrid EoSs shown in Fig. 1. The asterisks represent the last stable star of each model, having a zero frequency fundamental radial mode. As explained in Sec. 3, since we assume that quark-hadron phase conversions at the interface of a hybrid star have a slow timescale, there are parts of the curves that are dynamically stable in spite of having $\partial M/\partial \epsilon_c < 0$.

the compact star structure by means of the Tolman-Oppenheimer-Volkoff (TOV) equations, because some equilibrium quantities are needed during the numerical solution of the differential equations corresponding to the physics of tidal deformations.

The tidal Love number k_2 is found using the following expression (Hinderer 2008):

$$k_2 = \frac{8\mathcal{C}^5}{5} (1 - 2\mathcal{C})^2 [2 - y_R + 2\mathcal{C}(y_R - 1)] \times \{2\mathcal{C}[6 - 3y_R + 3\mathcal{C}(5y_R - 8)] + 4\mathcal{C}^3[13 - 11y_R + \mathcal{C}(3y_R - 2) + 2\mathcal{C}^2(1 + y_R)] + 3(1 - 2\mathcal{C})^2[2 - y_R + 2\mathcal{C}(y_R - 1)] \log(1 - 2\mathcal{C})\}^{-1} \quad (16)$$

where $\mathcal{C} \equiv M/R$ is the dimensionless compactness parameter and $y_R \equiv y(R)$, being $y(r)$ the solution of the following first-order differential equation (see Postnikov et al. (2010) for more details):

$$r \frac{dy(r)}{dr} + y(r)^2 + y(r)F(r) + r^2 Q(r) = 0. \quad (17)$$

In this equation, the coefficients are:

$$F(r) = [1 - 4\pi r^2(\epsilon - p)] \left[1 - \frac{2m}{r}\right]^{-1}, \quad (18)$$

$$Q(r) = 4\pi \left[5\epsilon + 9p + \frac{\epsilon + p}{c_s^2} - \frac{6}{4\pi r^2}\right] \left[1 - \frac{2m}{r}\right]^{-1} - \frac{4m^2}{r^4} \left[1 + \frac{4\pi r^3 p}{m}\right]^2 \left[1 - \frac{2m}{r}\right]^{-2}, \quad (19)$$

where $c_s^2 \equiv dp/d\epsilon$ is the squared speed of sound. The boundary condition for Eq. (17) at $r = 0$ is given by $y(0) = 2$. In summary, the tidal Love number can be obtained once an EoS is supplied and the TOV equations together with Eq. (17) are integrated.

5. IMPACT OF PHASE TRANSITIONS ON TIDAL POLARIZABILITY

Several models of NSs with first-order phase transitions have been recently analyzed (see e.g. Paschalidis et al. (2018); Nandi & Char (2018); Burgio et al. (2018); Christian et al. (2019); Sieniawska et al. (2019); Han & Steiner (2019); Montaña et al. (2019); Gomes et al. (2019); Mariani et al. (2019); Chatziioannou & Han (2020)).

In the presence of a finite energy density discontinuity, the last term in Eq. (19) involves a singularity $\propto (\epsilon + p)/c_s^2$. This was first discussed by Damour & Nagar (2009) addressing the surface vacuum discontinuity for incompressible stars. Postnikov et al. (2010)

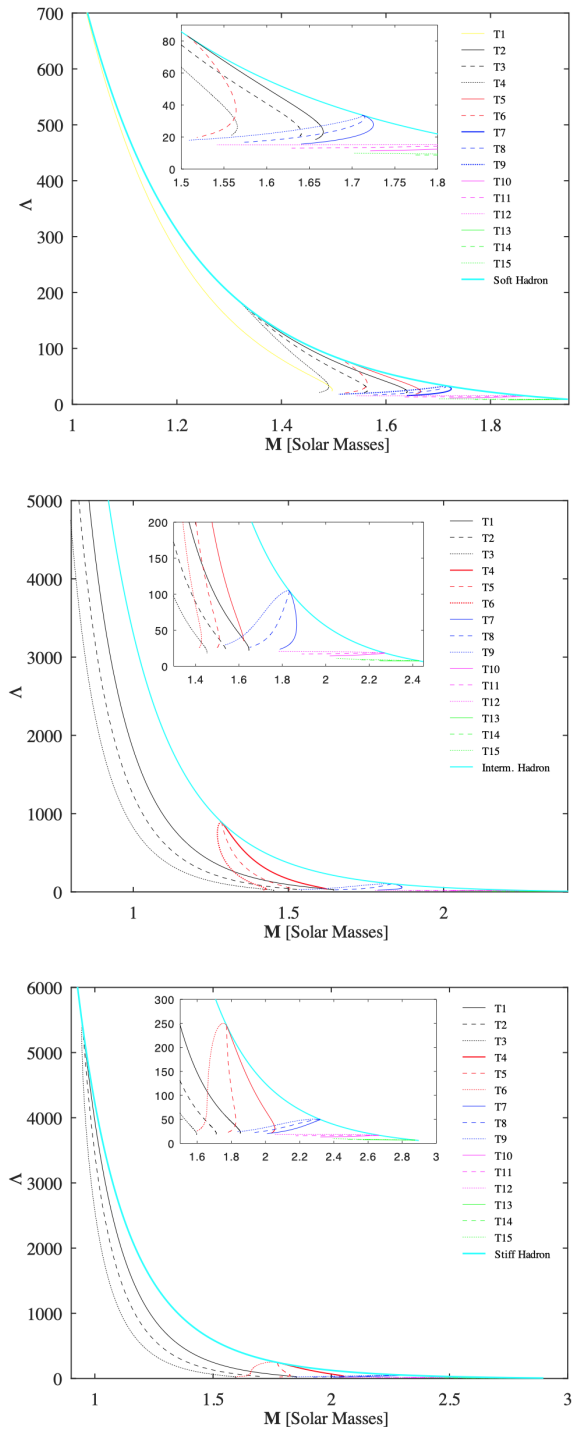


Figure 3. Tidal deformability Λ as a function of the stellar mass for the hybrid EoSs presented in Fig. 1.

extended this approach to the context of possible first-order transitions inside the stars. Therefore when there exists a first order transition inside the star, and additional junction condition for the $y(r)$ function has to be

imposed:

$$y(r_d + \epsilon) = y(r_d - \epsilon) - \Delta\rho/\tilde{\rho}, \quad (20)$$

where r_d represents the coordinate radius of the interface, i.e. the point where the phase transition takes place. The region $r < r_d$ represents the internal core containing quark matter and $r > r_d$ is the external hadronic region of the star. We also have that $\tilde{\rho} = m(r_d)/(4\pi r_d^3/3)$ and $\Delta\rho = \rho(r_d + \epsilon) - \rho(r_d - \epsilon)$.

The accumulated phase contribution due to the deformation from both of the stars is included in the inspiral signal as the combined dimensionless tidal deformability, which is given by

$$\tilde{\Lambda} = \frac{16}{13} \left[\frac{(m_1 + 12m_2)m_1^4\Lambda_1 + (m_2 + 12m_1)m_2^4\Lambda_2}{(m_1 + m_2)^5} \right], \quad (21)$$

where $\Lambda_1(m_1)$ and $\Lambda_2(m_2)$ are the tidal deformabilities of the individual binary components (Favata 2014). The quantity $\tilde{\Lambda}$ is usually evaluated as a function of the chirp mass $\mathcal{M}_c = (m_1 m_2)^{3/5}/(m_1 + m_2)^{1/5}$, for various values of the mass ratio $q = m_2/m_1$. From the event GW170817, it was possible to set the first upper limit on the dimensionless tidal deformability $\Lambda_{1.4}$ of a NS with a mass $1.4M_\odot$ such that $\Lambda_{1.4} \leq 800$ at 90% confidence level (for the case of low-spin priors) (Abbott et al. 2017). Independent of the waveform model or the choice of priors, the source-frame chirp mass was constrained to the range $\mathcal{M} = 1.188^{+0.004}_{-0.002} M_\odot$ and the mass ratio $q = m_2/m_1$ for low spin priors to the interval between 0.7 – 1.0 (Abbott et al. 2017). Working under the hypothesis that both NSs are described by the same EoS and have spins within the range observed in Galactic binary NSs, the tidal deformability $\Lambda_{1.4}$ of a $1.4M_\odot$ NS was estimated through a linear expansion of $\Lambda(m)m^5$ around $1.4M_\odot$ to be in the range 70 – 580 at the 90% level (Abbott et al. 2018).

In Fig. 3, we show the dimensionless tidal deformability Λ as a function of the stellar mass for all the hybrid models presented in Fig. 1. Notice that Λ is a decreasing function of M for the hadronic branch. However, for hybrid configurations, Λ can be either a decreasing or an increasing function of M . Moreover, for large values of the transition pressure, Λ shows a very weak dependence on the stellar mass (the curves are quite horizontal).

In Fig. 4, we show the dimensionless tidal deformabilities Λ_1 and Λ_2 for a binary NS system with the same chirp mass as GW170817. The curves are obtained as follows: once a value of m_1 is chosen one can calculate m_2 by fixing $\mathcal{M} = 1.188 M_\odot$. Running m_1 in the range of $1.36 \leq m_1/M_\odot \leq 1.60$ we obtain m_2 (with $1.17 \leq m_2/M_\odot \leq 1.36$). The values of Λ_1 and Λ_2 associated with m_1 and m_2 are depicted in Fig. 4.

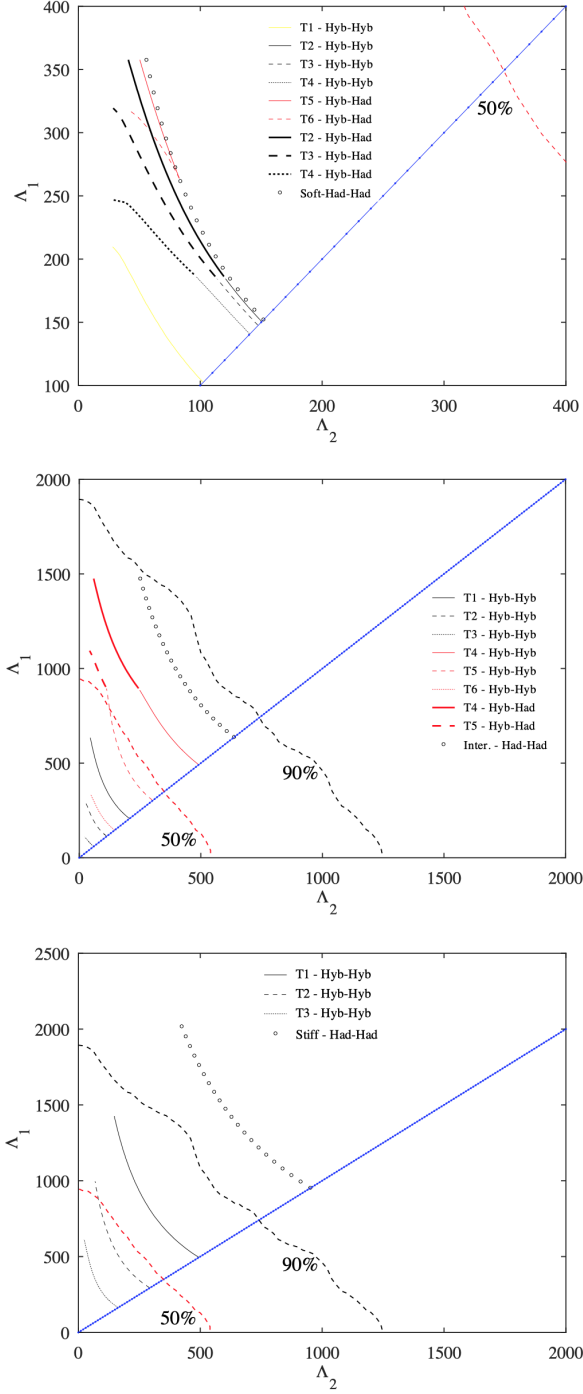


Figure 4. Dimensionless tidal deformabilities Λ_1 and Λ_2 for a binary NS system with masses m_1 and m_2 and the same chirp mass as GW170817 (Abbott et al. 2017). By definition we only plot combinations with $m_1 > m_2$. The diagonal blue line indicates the $\Lambda_1 = \Lambda_2$ boundary. The black dashed line denotes the 90% credibility level and the red dashed line the 50% level determined by LIGO/Virgo in the low-spin prior scenario.

We have analysed the three possibilities for the internal composition of the two stars in the binary system: hadron-hadron, hybrid-hadron and hybrid-hybrid. In the case with two purely hadronic stars, the presence of these binaries in the detection region depends strongly on the stiffness of the EoS. As can be seen in Fig. 4 the soft hadronic EoS is inside the 50% region of GW170817, the intermediate one is inside the 90% region and the stiff is outside the 90%. Note that the hybrid models that we do not show in Figure 4 are the cases that do not present hybrid configurations in the range $1.365 - 1.6 M_\odot$ (these cases are completely represented in the Λ_1 - Λ_2 plane by the hadronic curve with circle dots). In the scenario where at least one of the stars in the binary is hybrid, we find that only models T1, T2, T3, T4, T5 and T6 fall inside the detection region. Some of these curves have a lower part corresponding to hybrid-hybrid mergers and an upper part corresponding to hybrid-hadron mergers. There are also curves where the lower part represents hadron-hadron mergers and the upper part hybrid-hadron mergers. In general, we observe that as the density jump $\Delta\epsilon$ increases, the curves shift to lower values of Λ .

Notice that binary systems with at least one hybrid star that fall inside the area of the 90% credible region for Λ_1 - Λ_2 (T1, T2, T3, T4, T5 and T6) have maximum masses below $2 M_\odot$, and are therefore inconsistent with stringent constraints on the maximum NS mass coming from PSR J0348+0432 with $2.01 \pm 0.04 M_\odot$ (Antoniadis et al. 2013), PSR J0740+6620 with $2.14^{+0.10}_{-0.09} M_\odot$ (Cromartie et al. 2019), and PSR J2215-5135 with $2.27^{+0.17}_{-0.15} M_\odot$ (Linares et al. 2018). Therefore, for our model to agree with both the 90% level determined by LIGO/Virgo and the $2 M_\odot$ pulsars, both objects in GW170817 must be hadronic stars and hybrid configurations cannot fall in the range $1.365 - 1.6 M_\odot$. Viable candidates for this scenario would be the models from T7 to T15 linked to the hadronic EoS of *intermediate* stiffness. These models have $M_{\max} > 2 M_\odot$ (see central panel of Fig. 2) and are represented in the Λ_1 - Λ_2 plane by the hadronic curve with circle dots shown in the central panel of Fig. 4.

6. SUMMARY AND CONCLUSIONS

In this work we have analyzed hybrid stars that present sharp phase transitions between hadronic and quark matter assuming that phase conversions at the interface are slow. Hadronic matter has been described by the EoS presented by Hebeler et al. (2013) and quark matter by a generic bag model (Alford et al. 2005).

In the case of slow conversions at the quark-hadron interface, zero frequency radial modes happen in gen-

eral after the point of maximum mass, giving rise to an extended region of stable hybrid stars with central densities that are larger than the density of the maximum mass star (Pereira, Flores & Lugones 2018). This effect can be seen clearly in Fig. 2 where large extended branches arise. We have explored systematically the role of the transition pressure p_{tr} and the energy-density jump $\Delta\epsilon$ on the maximum mass object, the last stable configuration, and the tidal deformabilities. As expected, hybrid models with low enough p_{trans} are not able to reach a maximum mass above the observed value $M_{\text{max}} \approx 2M_{\odot}$. Also, for a given transition pressure, the radius of the last stable hybrid star decreases as $\Delta\epsilon$ raises resulting in a larger extended branch of stable hybrid stars (see Fig. 2).

We also find that for hybrid configurations, the tidal deformability Λ can be either a decreasing or an increasing function of M . Moreover, for large values of the transition pressure, Λ shows a very weak dependence on the stellar mass and the curves become almost horizontal in some cases (see Fig. 3). This is in contrast with the case of purely hadronic stars for which Λ is always a decreasing function of M .

Finally, we analyzed the tidal deformabilities Λ_1 and Λ_2 for a binary NS system with the same chirp mass as GW170817 (see Fig. 4). In the scenario where at least one of the stars in the binary is hybrid, we find

that only models with low enough transition pressure fall inside the 90% credible region for Λ_1 – Λ_2 . Unfortunately, these models have maximum masses below $2M_{\odot}$, i.e. in disagreement with the observation of PSR J0348+0432, PSR J0740+6620 and PSR J2215-5135. However, our model can explain the 90% level determined by LIGO/Virgo together with the $2M_{\odot}$ constrain if both objects in GW170817 are hadronic stars and all hybrid configurations have masses larger than $1.6M_{\odot}$. We find that several hybrid models involving the hadronic EoS of intermediate stiffness are in agreement with observations.

ACKNOWLEDGMENTS

Alessandro Parisi is grateful to Professor Feng-Li Lin for many helpful discussions. Germán Lugones is thankful to the Brazilian agency Conselho Nacional de Desenvolvimento Científico e Tecnológico (CNPq) for financial support. Csar H. Lenzi is thankful to the Fundao de Amparo Pesquisa do Estado de So Paulo (FAPESP) under thematic project 2017/05660-0 for financial support. Chian-Shu Chen is supported by Ministry of Science and Technology (MOST), Taiwan, R.O.C. under Grant No. 107-2112-M-032-001-MY3.

REFERENCES

- Abbott, B. P., Abbott, R., Abbott, T. D., et al. 2017, *PhRvL*, 119, 161101
- Abbott, B. P., Abbott, R., Abbott, T. D., et al. 2018, *PhRvL*, 121, 161101
- Abbott, R., Abbott, T. D., Abraham, S., et al. 2020, *ApJL*, 896, L44
- Alford, M., Braby, M., Paris, M., et al. 2005, *ApJ*, 629, 969
- Alford, M. G., Han, S., & Prakash, M. 2013, *PhRvD*, 88, 083013
- Alford, M. G., Burgio, G. F., Han, S., et al. 2015, *PhRvD*, 92, 083002
- Alford, M., & Sedrakian, A. 2017, *PhRvL*, 119, 161104
- Annala, E., Gorda, T., Kurkela, A., et al. 2018, *PhRvL*, 120, 172703
- Antoniadis, J., Freire, P. C.C., Wex, N., et al. 2013, *Science*, 340, 448
- Baym, G., Hatsuda, T., Kojo, T., et al. 2018, *Reports on Progress in Physics*, 81, 056902
- Baym, G., Pethick, C., & Sutherland, P. 1971, *ApJ*, 170, 299
- Benić, S., Blaschke, D., Alvarez-Castillo, D.E., et al. 2015, *A&A*, 577, A40
- Biswas, B., Nandi, R., Char, P., et al. 2019, *PhRvD*, 100, 044056
- Buballa, M., Dexheimer, V., Drago, A., et al. 2014, *Journal of Physics G Nuclear Physics*, 41, 123001
- Burgio, G. F., Drago, A., Pagliara, G., et al. 2018, *ApJ*, 860, 139
- Carson, Z., Steiner, A. W., & Yagi, K. 2019, *PhRvD*, 99, 043010
- Chatziioannou, K., & Han, S. 2020, *PhRvD*, 101, 044019
- Christian, J.-E., Zacchi, A., & Schaffner-Bielich, J. 2018, *European Physical Journal A*, 54, 28
- Christian, J.-E., Zacchi, A., & Schaffner-Bielich, J. 2019, *PhRvD*, 99, 023009
- Cromartie H. T., Ransom S. M., Demorest P. B. et al. 2019, *Nature Astron.* 4, 72
- Damour, T., & Nagar, A. 2009, *PhRvD*, 80, 084035
- De, S., Finstad, D., Lattimer, J. M., et al. 2018, *PhRvL*, 121, 091102
- Demorest, P. B., Pennucci, T., Ransom, S. M., et al. 2010, *Nature*, 467, 1081
- Endo, T. 2011, *PhRvC*, 83, 068801

- Farhi, E., & Jaffe, R. L. 1984, *PhRvD*, 30, 2379
- Fattoyev, F. J., Piekarewicz, J., & Horowitz, C. J. 2018, *PhRvL*, 120, 172702
- Fattoyev F. J., Carvajal J., Newton W. G., Li B. A., 2013 *PhRvC*, 87, 015806 (2013).
- Favata, M. 2014, *PhRvL*, 112, 101101
- Flanagan E. E, Hinderer T., 2008, *PhRvD*, 77, 021502
- Flanagan, É. É., & Hinderer, T. 2008, *PhRvD*, 77, 021502
- Flores, C. V., Lenzi C. H. and Lugones, G. 2012, *Int. J. Mod. Phys. Conf. Ser.* **18**, 105-108.
- Gerlach, U. H. 1968, *Physical Review*, 172, 1325
- Glendenning, N. K., & Kettner, C. 2000, *A&A*, 353, L9
- Gomes, R. O., Char, P., & Schramm, S. 2019, *ApJ*, 877, 139
- Han, S., & Steiner, A. W. 2019, *PhRvD*, 99, 083014
- Hebeler, K., Lattimer, J. M., Pethick, C. J., et al. 2013, *ApJ*, 773, 11
- Hinderer, T. 2008, *ApJ*, 677, 1216
- Hinderer T., Lackey B. D., Lang R. N., Read J. S., 2010, *PhRvD*, 81, 123016
- Hornick N., Tolos L., Zacchi A., Christian J. E., Schaffner-Bielich J., 2018, *PhRvC*, 98, 065804
- Iida, K., & Sato, K. 1998, *PhRvC*, 58, 2538
- Itoh, N. 1970, *Progress of Theoretical Physics*, 44, 291
- Ivanenko, D. D., & Kurdgelaidze, D. F. 1965, *Astrophysics*, 1, 251
- Kaltenborn, M. A. R., Bastian, N.-U. F., & Blaschke, D. B. 2017, *PhRvD*, 96, 056024
- Kampfer, B. 1983, *Journal of Physics G Nuclear Physics*, 9, 1487
- Kim, Y.-M., Lim, Y., Kwak, K., et al. 2018, *PhRvC*, 98, 065805
- Krastev, P. G., & Li, B.-A. 2019, *Journal of Physics G Nuclear Physics*, 46, 074001
- Kumar B., Biswal S. K., Patra S. K., 2017, *PhRvC*, 95, 015801
- Lattimer, J. M. 2012, *Annual Review of Nuclear and Particle Science*, 62, 485
- Lattimer, J. M., & Prakash, M. 2016, *PhR*, 621, 127
- Lau, S. Y., Leung, P. T., & Lin, L.-M. 2019, *PhRvD*, 99, 023018
- Li, J. J., & Sedrakian, A. 2019, *ApJL*, 874, L22
- Linares M., Shahbaz T. and Casares J., 2018, *Astrophys. J.* 859, 54
- Lourenço, O., Dutra, M., Lenzi, C. H., et al. 2020, *European Physical Journal A*, 56, 32
- Lourenço, O., Dutra, M., Lenzi, C. H., et al. 2019, *PhRvC*, 99, 045202
- Lugones, G., Grunfeld, A. G., & Ajmi, M. A. 2013, *PhRvC*, 88, 045803
- Lugones, G. & Grunfeld, A. G. 2017, *Phys. Rev. C* 95, 015804
- Lugones, G. 2016, *Eur. Phys. J. A* 52, 53
- Lugones, G. & Grunfeld, A. G. 2019, *Phys. Rev. C* 99, 035804
- Malik, T., Alam, N., Fortin, M., et al. 2018, *PhRvC*, 98, 035804
- Mannarelli, M., Pagliaroli, G., Parisi, A., et al. 2014, *PhRvD*, 89, 103014
- Mannarelli, M., Pagliaroli, G., Parisi, A., et al. 2015, *ApJ*, 815, 81
- Mariani, M., Orsaria, M. G., Ranea-Sandoval, I. F. and Lugones, G. 2019, *MNRAS*, 489, 4261
- Maruyama T., Chiba S., Schulze H.-J., Tatsumi T. 2007, *Phys.Rev. D* 76, 123015
- Miller, M. C., Lamb, F. K., Dittmann, A. J., et al. 2019, *ApJL*, 887, L24
- Montaña, G., Tolós, L., Hanauske, M., et al. 2019, *PhRvD*, 99, 103009
- Most, E. R., Weih, L. R., Rezzolla, L., et al. 2018, *PhRvL*, 120, 261103
- Most, E. R., Papenfort, L. J., Dexheimer, V., et al. 2019, *PhRvL*, 122, 061101
- Nandi, R., Char, P., & Pal, S. 2019, *PhRvC*, 99, 052802
- Nandi, R., & Char, P. 2018, *ApJ*, 857, 12
- Negele, J. W., & Vautherin, D. 1973, *NuPhA*, 207, 298
- Pacini, F. 1966, *Nature*, 209, 389
- Paschalidis, V., Yagi, K., Alvarez-Castillo, D., et al. 2018, *PhRvD*, 97, 084038
- Penner, A. J., Andersson, N., Samuelsson, L., et al. 2011, *PhRvD*, 84, 103006
- Pereira, J. P., Flores, C. V., & Lugones, G. 2018, *ApJ*, 860, 12
- Pereira, J. P., Bejger, M., Andersson, N., et al. 2020, *ApJ*, 895, 28
- Pinto, M. B., Koch, V., & Randrup, J. 2012, *PhRvC*, 86, 025203
- Postnikov, S., Prakash, M., & Lattimer, J. M. 2010, *PhRvD*, 82, 024016
- Poisson E., 2009, *PhRvD*, 80, 084018
- Raithel, C. A., Özel, F., & Psaltis, D. 2018, *ApJL*, 857, L23
- Ranea-Sandoval, I. F., Han, S., Orsaria, M. G., et al. 2016, *PhRvC*, 93, 045812
- Riley, T. E., Watts, A. L., Bogdanov, S., et al. 2019, *ApJL*, 887, L21
- Schertler, K., Greiner, C., Schaffner-Bielich, J., and Thoma, M. H. 2000 *Nucl. Phys. A* **677** 463
- Sieniawska, M., Turczański, W., Bejger, M., et al. 2019, *A&A*, 622, A174

- Souza, L. A., Dutra, M., Lenzi, C. H., et al. 2020, PhRvC, 101, 065202
- Tews, I., Margueron, J., & Reddy, S. 2018, PhRvC, 98, 045804
- Tsang, C. Y., Tsang, M. B., Danielewicz, P., et al. 2019, Physics Letters B, 796, 1
- Vásquez Flores, C., Parisi, A., Chen, C.-S. & Lugones, G. 2019, JCAP, 2019, 051
- Voskresensky D. N. , Yasuhira M. , Tatsumi T. 2003, Nucl. Phys. A 723, 291
- Zhao, T., & Lattimer, J. M. 2018, PhRvD, 98, 063020
- Zhou, E.-P., Zhou, X., & Li, A. 2018, PhRvD, 97, 083015